Eleventh International Conference on CFD in the Minerals and Process Industries
CSIRO, Melbourne, Australia
7-9 December 2015

BROWNIAN DYNAMICS OF NANO-FIBERS IN HUMAN UPPER TRACHEOBRONCHIAL AIRWAYS

Lin TIAN[1*], Goodarz AHMADI[2] and Jiyuan TU[1]

[1] School of Aerospace, Mechanical and Manufacturing, RMIT University, Bundoora, VIC, AUSTRALIA
[2] Mechanical and Aeronautical Engineering, Clarkson University, Potsdam, NY, USA

*Corresponding author, E-mail address: lin.tian@rmit.edu.au

ABSTRACT

Transport and deposition of inhaled asbestos fibers has been studied in the past few decades due to its pathological response in living being. In the earlier studies, in vitro and vivo experiments in human and animal subjects were reported; however, the reported computational studies are sparse. In this work, the transport and deposition of nano-fibers were simulated in a physiologically realistic lung bifurcation model. Focus of this study was to explore the effect of the Brownian dynamics on the very thin fibers, and how it affects the transport and deposition of the fibers in human airway passages. Motion of the inhaled fibers and their interactions with the surrounding environment were reproduced by solving the system of coupled nonlinear equations governing the fiber translational and rotational motions. Hydrodynamic drag and torque, turbulence dispersion, gravitational sedimentation, and the Brownian diffusion were accounted for. The study uncovered the very important role of Brownian dynamics in thin fibers' motion in human tracheobronchial airways. The simulation results were compared with the experimental measurements, and the carcinogenicity of these fibers in human airways was discussed. The simulation results can help explain many of the earlier experimental findings.

NOMENCLATURE

f^B Brownian diffusion force
f^h hydrodynamic drag
f^L shear induced life
g gravitational acceleration
$(I_{\hat{x}}, I_{\hat{y}}, I_{\hat{z}})$ momentum of inertia in the fiber coordinate
k turbulence kinetic energy
m^p mass of the fiber
$\bar{p}$ mean fluid pressure
P_{ij} turbulence production
R_{ij} Reynolds stress tensor
t time
$(T^B_{\hat{x}}, T^B_{\hat{y}}, T^B_{\hat{z}})$ Brownian diffusion torque in the fiber coordinate
$(T^h_{\hat{x}}, T^h_{\hat{y}}, T^h_{\hat{z}})$ hydrodynamic torque in the fiber coordinate
$\bar{u}_i$ mean fluid velocity
u_i fluid fluctuation velocity
u^* turbulence shear velocity
v fiber centroid velocity vector
$(\omega_{\hat{x}}, \omega_{\hat{y}}, \omega_{\hat{z}})$ angular velocity in the fiber coordinate
x_i Eulerian position
ε turbulence dissipation rate
ρ density of fluid
ν fluid kinematic viscosity
ν_T turbulence eddy viscosity

INTRODUCTION

Occupational exposure to asbestos fibers has been linked to the occurrence of malignant respiratory diseases such as mesothelioma and lung cancer. It is now widely accepted, the respiratory pathological response in living being is mainly induced by the retention and deposition of the inhaled asbestos fibers. Measurements of such deposition in human patient tissues as well as in vivo animal studies were reported by many researchers, such as Lippmann et al. (1988, 1990), Berman et al. (1995), and Suzuki et al. (2005). Based on the available data EPA (2003) concluded that fibers with length shorter than 5 μm posed minimum risk, while the threshold for diameter needed further investigation. NIOSH (2008) concluded that fibers with length smaller than 1.5 μm or greater than 40 μm and diameter thinner than 0.25 μm or thicker than 3 μm, respectively, were at the highest risk to cause lung cancer.

In this study, simulation of the transport and deposition of elongated ellipsoidal fibers in the first generation of human airway model was conducted. Mathematical description of fiber motion was given by system of coupled nonlinear equations accounting for the hydrodynamic drag and torque, shear induced lift, Brownian diffusion, and the gravitational sedimentation. The simulated results provided detailed information for analyzing the contribution of fiber dimensional characteristics (length, diameter, aspect ratio, density) toward deposition. Effects of the airflow pattern and airway morphology were also studied. For a dilute suspension, the one-way coupling assumption was used, and an in-house C++ code was developed as post processing for the FLUENT-ANSYS code (FLUENT, 1998), for analysing the inhaled fiber movements. Results of the study were compared to earlier experimental measurements, and carcinogenicity of the fiber in relation to its dimensional characteristics was discussed.

COMPUTATIONAL MODEL

Fiber Model

For the ellipsoidal fiber shown in Figure 1, the governing equations for the coupled translational and rotational motion are:

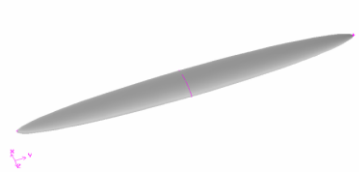

Figure 1: Schematic diagram of ellipsoidal fiber.

$$m^p \frac{d\mathbf{v}}{dt} = m^p \mathrm{g} + \mathrm{f}^h + \mathrm{f}^L + f^B, \quad (1)$$

$$I_{\hat{x}} \frac{d\omega_{\hat{x}}}{dt} - \omega_{\hat{y}}\omega_{\hat{z}}(I_{\hat{y}} - I_{\hat{z}}) = T_{\hat{x}}^h + T_{\hat{x}}^B, \quad (2)$$

$$I_{\hat{y}} \frac{d\omega_{\hat{y}}}{dt} - \omega_{\hat{z}}\omega_{\hat{x}}(I_{\hat{z}} - I_{\hat{x}}) = T_{\hat{y}}^h + T_{\hat{y}}^B, \quad (3)$$

$$I_{\hat{z}} \frac{d\omega_{\hat{z}}}{dt} - \omega_{\hat{x}}\omega_{\hat{y}}(I_{\hat{x}} - I_{\hat{y}}) = T_{\hat{z}}^h + T_{\hat{z}}^B \quad (4)$$

Here **v** is the velocity vector of the fiber particle mass center in the fixed coordinate, and $(\omega_{\hat{x}}, \omega_{\hat{y}}, \omega_{\hat{z}})$ is the angular velocity vector of the fiber in the particle frame (Cartesian coordinate attached to the fiber centroid with its axes parallel to the fiber's principle axis). m^p is the mass of the fiber, ***g*** is the acceleration of gravity, $\boldsymbol{f}^h$ is the hydrodynamic force, and $\boldsymbol{f}^L$ is the shear induced lift force. $(\mathrm{I}_{\hat{x}}, \mathrm{I}_{\hat{y}}, \mathrm{I}_{\hat{z}})$ is the moments of inertia of the fiber about the principle axes in the particle frame $(\hat{\mathrm{x}}, \hat{\mathrm{y}}, \hat{\mathrm{z}})$, $(\mathrm{T}_{\hat{x}}^h, \mathrm{T}_{\hat{y}}^h, \mathrm{T}_{\hat{z}}^h)$ and $(T_{\hat{x}}^B, T_{\hat{y}}^B, T_{\hat{z}}^B)$ are the hydrodynamic torques and Brownian torque acting on the particle with respect to the principle axes in the particle frame.

Airway Bifurcation Model

It is known that the branching pattern of the human tracheobronchial tree is highly asymmetric (Phillips & Kaye, 1997). The asymmetry of the bifurcation significantly affects the partition of the volume flow rate between the daughter branches. Based on the description of Phillips and Kaye (1997) and Heistracher and Hofmann (1995), a two-branch single asymmetric bifurcation model is developed as shown in Fig. 2. Table 1 details the parameters for the first bifurcation including the trachea and the main left and right bronchus (G0 and G1).

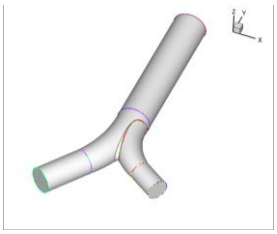

Figure 2: Schematic diagram of the trachea and the first bifurcation.

Computational Mesh

Due to the advantage of unstructured mesh generation and its flexibility in being adapted to complex geometries, unstructured tetrahedral elements are selected. A key component of the mesh quality is the ability to resolve the near wall turbulence fluctuating scales when the flow is turbulent. A highly refined boundary layer with $y^+ = 1$ being the first grid point in the boundary normal direction is attached to the wall suggested by the "two-layer zonal model" boundary condition (Tian and Ahmadi, 2007). Tetrahedral elements with cell dimension of 1 mm are used for the fully developed core region, while, near the wall, a highly dense layer of hexahedron elements in the wall normal direction is generated. This dense layer evolves from the first grid point at $y^+ = 1$ (cell dimension of 0.05 mm) to the core region with a growing factor 1.2. The resulting asymmetric tracheobronchial bifurcation model (G0 to G1) consists of 550,658 elements. The mesh is generated with the software package Gambit 2.3.16 (Fig. 3). Grid independency is conducted and verified.

Location	Diameter (m)	Length (m)	BA/RC	BFRC
Trachea	0.02	0.08	--	0.0016
Bron. (a)	0.016	0.03	35/0.0752	--
Bron. (b)	0.0128	0.018	55/0.0455	--

* BA – branching angle * RC – radius of curvature * BFRC – bifurcation radius of curvature.

Table 1. Geometry specifications of the two-branch asymmetric bifurcation model

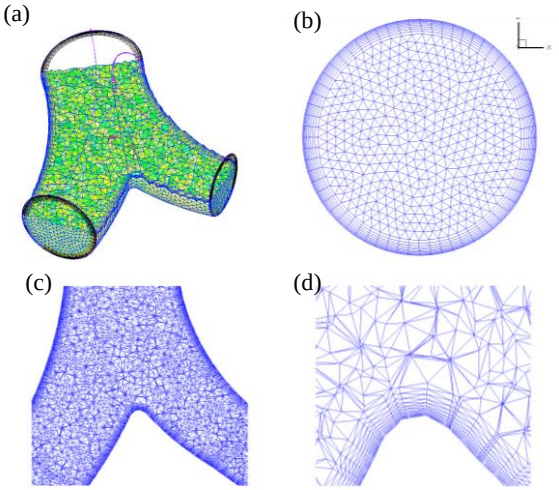

Figure 3: Computational grid: (a) Schematic view inside the airway bifurcation. (b) Surface mesh at the inlet. (c) Mesh plane view of the bifurcation. (d) Mesh near the vicinity of the carinal ridge.

Airflow Simulation

Due to larynx-induced disturbance, the airflow in human upper tracheobronchial airways is in turbulent state of motion. In deeper airways (beyond the third generation) turbulence dies down and laminar flow prevails. In this study, the first generation is considered where a Reynolds stress transport model in the core and a turbulence two-layer zonal model at the boundary are employed for the mean flow profile.

Under normal breathing conditions, the air behaves as an incompressible fluid. The corresponding governing equations of the mean flow are given as:

$$\frac{\partial \bar{\mathrm{u}}_\mathrm{i}}{\partial \mathrm{x}_\mathrm{i}} = 0 \quad (5)$$

$$\frac{\partial \bar{u}_i}{\partial t} + \bar{u}_j \frac{\partial \bar{u}_i}{\partial x_j} = -\frac{1}{\rho}\frac{\partial \bar{p}}{\partial x_i} + \nu \frac{\partial^2 \bar{u}_i}{\partial x_j \partial x_j} - \frac{\partial}{\partial x_j} R_{ij} \qquad (6)$$

Here $\bar{u}_i$ is the mean fluid velocity, x_i is Eulerian position, $\bar{p}$ is the mean pressure, ρ is the constant mass density of fluid, ν is the fluid kinematic viscosity, $R_{ij} = \overline{u_i' u_j'}$ is the Reynolds stress tensor, and u_i' is the fluctuation velocity. The corresponding instantaneous velocity is then given as $u_i = \bar{u}_i + u_i'$.

The transport equation for the Reynolds stress tensor R_{ij} is given by:

$$\frac{\partial}{\partial t} R_{ij} + \bar{u}_k \frac{\partial}{\partial x_j} R_{ij} = \frac{\partial}{\partial x_k}\left(\frac{\nu_T}{\sigma^k}\frac{\partial}{\partial x_k} R_{ij}\right) - [\overline{u_i' u_k'}\frac{\partial \bar{u}_j}{\partial x_k} + \overline{u_j' u_k'}\frac{\partial \bar{u}_i}{\partial x_k}]$$
$$- C_1 \frac{\varepsilon}{k}[R_{ij} - \frac{2}{3}\delta_{ij} k] - C_2 \frac{\varepsilon}{k}[P_{ij} - \frac{2}{3}\delta_{ij} P] - \frac{2}{3}\delta_{ij}\varepsilon. \qquad (7)$$

In Eq. (7), P_{ij} is the turbulence production, $P = P_{ii}/2$. The standard values of the constants are $\sigma^k = 1.0$, $C_1 = 1.8$, and $C_2 = 0.6$ (Launder et al., 1975). These values of constants lead to the proper values of $\overline{u_1'^2}$, but overestimate $\overline{u_2'^2}$. He and Ahmadi (1999) suggested using $C_1 = 1.5$ and $C_2 = 0.1$ for the proper estimation of $\overline{u_2'^2}$.

The transport equation for the turbulence dissipation rate is given as:

$$\frac{d\varepsilon}{dt} = \frac{\partial}{\partial x_j}\left(\frac{\nu_T}{\sigma_\varepsilon}\frac{\partial \varepsilon}{\partial x_j}\right) + c_{\varepsilon 1}\nu_T \frac{\varepsilon}{k}\left(\frac{\partial \bar{u}_i}{\partial x_j} + \frac{\partial \bar{u}_j}{\partial x_i}\right)\frac{\partial \bar{u}_i}{\partial x_j} - c_{\varepsilon 2}\frac{\varepsilon^2}{k} \qquad (8)$$

Here, $\nu_T = c_\mu k^2/\varepsilon$ is the eddy viscosity, and $k = \overline{u_i' u_i'}/2$ is the turbulence kinetic energy. The standard values of the constants in the dissipation equation are $c_\mu = 0.09$, $c_{\varepsilon 1} = 1.45$, $c_{\varepsilon 2} = 1.9$, and $\sigma_\varepsilon = 1.3$ (Jones & Launder, 1973).

Here the Reynolds stress transport model is used due to its relative simplicity and computational efficiency. More important the anisotropic feature is superior, in the particle deposition study, than other isotropic turbulence models such as k-ε/k-ω models. Details of the comparative study of particle transport and deposition by using different turbulence models can be found in the work of Tian and Ahmadi (2007).

The Filter White Noise (CFWN) Model with normal quadratic fluctuation correction is used to reproduce the turbulence fluctuations in the passage and near the walls (Tian and Ahmadi, 2007).

Boundary Conditions

The inhaled air properties in the simulations are air temperature T = 300 K, dynamic viscosity $\mu = 1.84 \times 10^{-5}$ Ns/m^2, and air density $\rho = 1.125$ kg/m3. Breathing rate of 15, 40 and 60 L/min, representing light, medium and heavy cardiac load, is considered in the analysis. A uniform flow is imposed at the trachea entrance, and rigid airway surface is assumed. The disturbance of the larynx jet is introduced by prescribing turbulence intensities at the trachea inlet. Carbon fibers with a density of 1830 kg/m3 and diameter of 1 nm to 3.66 μm, with a range of aspect ratios from 4 to 300 are included in these simulations. Gravity is in the negative y direction. While it is highly unlikely that fibers of 3 mm length pass through the nasal barrier, the simulations include this group of fibers for comparative study. Fiber initial velocity is set equal to zero. The "trap" wall boundary condition for fiber-wall interaction is used. This implies that the fiber will stick to the wall upon contact. Typically 3000 fibers are released with a uniform distribution at the trachea entrance. When entering the airway, the fibers are assumed to be initially parallel to the flow direction.

RESULTS

Figure 4 displays the simulated fiber motion in the trachea and the first bifurcation for a breathing rate of 40 L/min. Diameter of the fiber is 0.1 μm, while lengths of the fiber are, respectively, 0.4 μm, 1.2 μm and 2.4 μm, or aspect ratio of 4, 12 and 24. Throughout the trajectory, fibers illustrate coupled translational and rotational motion. Distinctive Brownian excitation is observed in Figure 4.a while smoother motion is exhibited for longer fibers (Figure 4.b and 4.c). It is shown in Figure 4.c that longer fibers tend to suppress the rotation; this may have profound effect in predicting fiber deposition rate.

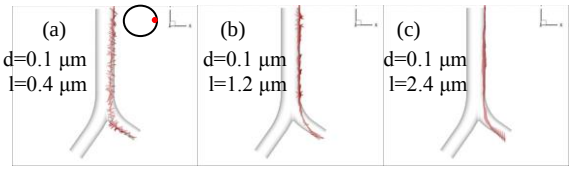

Figure 4: Simulated fiber motion.

Figure 5 displays the simulated fiber deposition pattern for a breathing rate of 40 L/min. Figure 5.a and 5.b present the result for fibers with diameter being 3.66 μm and aspect ratio being 15 and 80, while Figure 5.c and 5.d show the result for fibers with diameter of 0.1 μm and aspect ratio of 15 and 80. It is seen from Figure 5.a and 5.b that most of the depositions occur at the bifurcation and the inner ridge of the daughter branches. This indicates that the major deposition mechanism is inertial deposition. However in Figure 5.c and 5.d, the deposition is more uniformly distributed at the bifurcation as well as at the outer wall of the daughter branches. This implies a diffusion deposition mechanism. In summary, fiber deposition pattern in the human upper airways is largely affected by the transport mechanism. For ellipsoidal fibers, the deposition mechanism is determined by its diameter. For fibers with diameter larger than 3.66 μm, inertial impaction plays the major role, while for fibers with diameter 0.1 μm or smaller, diffusion is the major deposition mechanism.

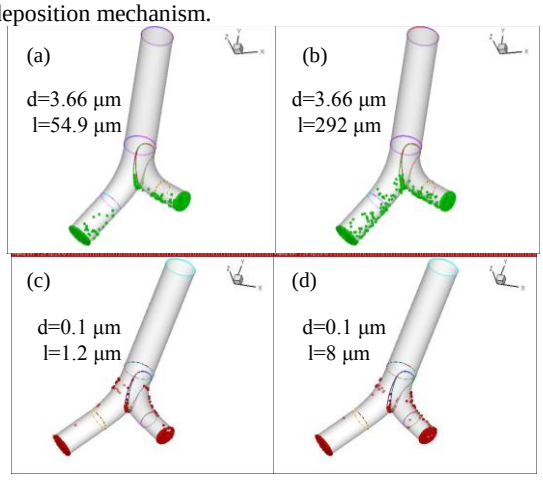

Figure 5: Simulated fiber deposition pattern.

Figure 6 compares the predicted fiber deposition efficiency in the trachea and the first bifurcation. The data are plotted versus the equivalent fiber relaxation time. Experimental measurements of Zhou et al. (2007) in a human airway replica are plotted in this figure for comparison. Carbon fibers of semi-minor being 3.66 μm, and aspect ratios from 1 to 80 are included in the simulation study. It is observed from Figure 6 that the measured deposition rates are rather scattered. For the inertial size range considered, in general, as the fiber relaxation time increases, the deposition efficiency increases. The fiber deposition is also enhanced as the breathing rate increases. However, at moderate to intensive breathing rates (40 to 60L/min), the effect of the airflow on the fiber deposition is less important. According to Tian and Ahmadi (2007), the near wall correction on the turbulence fluctuation near a surface is essential for correct prediction of the particle deposition rates in turbulent flows. The present simulation accounts for this correction by using the turbulence near wall "two-layer zonal model" and the "quadratic variation near wall model". A series of simulations for wall corrections being made assuming a range of u* are performed and the results are presented in Figure 6. This figure shows that altering the level of shear velocity (u*) for the near wall correction will affect the fiber deposition rates noticeably. Higher values of shear velocity lead to higher values of turbulence fluctuations and leads to higher deposition rate. Figure 6 shows that for the range of u* considered, the predicted deposition rate are within the range of the experimental measurements. This figure further shows the importance of the turbulence near wall correction in the study of fiber depositions in human lung. Due to the complexity of fiber deposition and the scatter of the experimental data, the applied correction as quantified by the values of u* appears to be reasonable.

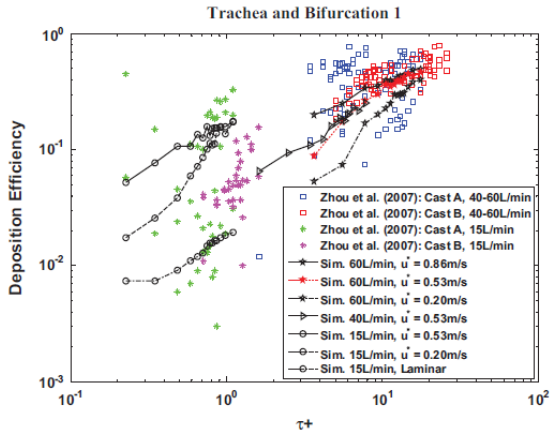

Figure 6: Comparison of Simulated Fiber Deposition Efficiency.

CONCLUSIONS

The computational model is able to reproduce the coupled fiber motion in human upper tracheobronchial airways covering from inertial to Brownina region. The Brownian diffusion is successfully simulated and it is shown to have profound effect on the movement of fibers with extremely thin diameters (d < 0.1 μm). Intensive Brownian rotation is observed for fibers with small aspect ratio (length); however, longer fibers of this group tend to overcome the Brownian excitation and stay aligned with the flow with less rotational oscillation. Inertial and diffusion deposition patterns for large and extra thin fibers are also illustrated. Finally, the simulated deposition efficiency agrees well with the experimental data. This suggests the developed computational model is suitable for simulating the fiber transport and depositions in the human tracheobronchial airways.

ACKNOWLEDGEMENTS

This work is supported by National Institute for Occupational Safety and Health (NOISH) and Center for Air Resources Engineering and Science at Clarkson University.

REFERENCES

BERMAN, D.W., CRUMP, K.S., CHATFIELD, E.J., DAVIS, J.M.G. AND JONES, A.D., (1995), "The sizes, shapes, and mineralogy of asbestos structures that induce lung tumors or mesothelioma in AF/HAN rats following inhalation", *Risk Anal.*, **15**, 188–195.

EPA (U.S. Environmental Protection Agency). 2003.

FLUENT User's Guide, (1998), Fluent Inc., Lebanon, NH.

HE, C. AND AHMADI, G., (1999), "Particle deposition in a nearly developed turbulent duct flow with electrophoresis", *Journal of Aerosol Science*. **30**, 739-758.

HEISTRACHER, T., AND HOFMANN, W., (1995), "Physiological realistic models of bronchial airway bifurcations". *Journal of Aerosol Science*, **26**, 497-509.

JONES, W.P. AND LAUNDER B.E., (1973), "The calculation of low Reynolds number phenomena with a two-equation model of turbulence", *International Journal of Mass Heat Transfer*, **16**, 1119-1130.

LIPPMANN, M.,(1988), "Asbestos exposure indices", *Environ Res*., **46**, 86–106.

LIPPMANN, M., (1990), "Effects of fiber characteristics on lung deposition, retention, and disease", *Environ Health Perspect*. **88**, 311–317.

LAUNDER, B.E., REECE, G.J. AND RODI, W., (1975), "Progress in the development of a Reynolds-stress turbulent closure", *Journal of Fluid Mechanics*. **68**, part3, 537-566.

NIOSH (National Institute for Occupational Safety and Health), 2005.

PHILLIPS, C.G., AND KAYE, S.R., (1997), "On the asymmetry of bifurcations in the bronchial tree", *Respiration Physiology*, **107**, 85-98.

SUZUKI, Y., YUEN, S. AND ASHLEY, R., (2005), "Short thin asbestos fibers contribute to the development of human malignant mesothelioma: pathological evidence", *Int J Hyg Environ Health*, **208**, 201–210.

TIAN, L. AND AHMADI, G., (2007), "Particle deposition in turbulent duct flows – comparisons of different model predications", *Journal of Aerosol Science*, **38**, 377–397.

ZHOU, Y., SU, W-C. AND CHENG, Y.S., (2007), "Fiber deposition in the tracheabronhical region: experimental measurements", *Inhalation Toxicology*, **19**, 1071–1078.